High-Resolution Metabolic Imaging of Human Breast Cancer

Charles S Springer, Jr. [1], Xin Li[1], Luminita A. Tudorica[2], Karen Y. Oh[2], Nicole Roy[2], Stephen Y-C. Chui[3], Arpana M. Naik[4], Megan L. Holtorf[5], Aneela Afzal[1], William D. Rooney[1], and Wei Huang[1]

[1]Advanced Imaging Research Center, Oregon Health & Science University, Portland, Oregon, United States, [2]Diagnostic Radiology, Oregon Health & Science University, Portland, Oregon, United States, [3]Hematology/Oncology, Oregon Health & Science University, Portland, Oregon, United States, [4]Surgical Oncology, Oregon Health & Science University, Portland, Oregon, United States, [5]Clinical Trials Office, Oregon Health & Science University, Portland, Oregon, United States

Introduction: The use of the tracer pharmacokinetic paradigm for DCE-MRI is incorrect. All tracer expressions presume the signal has no information on tracer compartmentalization. In DCE-MRI, however, the contrast agent [CA] is the tracer molecule but water is the signal molecule: CA compartmentalizations are intrinsic to the DCE ^1H_2O signal time-course. This requires the shutter-speed [SS] pharmacokinetic paradigm (1). ROI-averaged SS DCE-MRI parameters allow better specificity in breast (2) and prostate (1,3) cancer detection and in breast therapy prediction (4). However, recent findings of intra-tumor phylogenetic heterogeneity (5) and its metabolic consequences (6) provide challenges for: blood tests, point biopsies, *ex vivo* tissue homogenization, and for ROI- and population-averaged imaging biomarkers. A premium is placed on individualized *in vivo* metabolic imaging, with intra-tumor resolution generally unattainable. Since SS DCE-MRI yields the metabolic biomarker τ_i [the mean intracellular water lifetime], it allows metabolic imaging with ^1H_2O MR spatial resolution. For in-depth analyses, we take two representative human breast cancer [neoadjuvent chemotherapy] NACT case studies from a larger population. The subjects are their own controls.

Methods: The patients [grade 2 IDC, HER2-pos, BRCA1/BRCA2-neg] consented to research DCE-MRI at [therapy point] TP_0 - before NACT and TP_1 - after first 3 week NACT cycle, as well as other points during and after the NACT course, usually 6 cycles. Axial bilateral DCE-MRI with fat-saturation and full breast coverage was acquired [3D GE-based TWIST (7)] at 3T [Siemens]. The parameters included 10° flip angle, 2.9/6.2 ms TE/TR, a parallel imaging acceleration factor of 2, 30-34 cm FOV, 320x320 matrix size, and 1.4 mm slice thickness. The total acquisition time was ~ 10 min for 32-34 image volume sets with 18-20 s temporal resolution. CA (Prohance®) IV injection (0.1 mmol/kg at 2 mL/s) was timed to start following acquisitions of two baseline image volumes. Inclusive tumor ROIs were drawn by experienced radiologists. The pixel-by-pixel (within the ROI) DCE time-course data were subjected to SS pharmacokinetic analyses to extract K^{trans}, v_e, and τ_i. [K^{trans} is mainly a rate constant for capillary CA extravasation/tissue arrival, and v_e the CA distribution volume (interstitium) fraction.] Response to NACT and residual cancer burden (RCB) for each patient were determined by pathology analysis of post-therapy resection specimens and comparison with pre-therapy core biopsy specimens.

Results: **Figure 1** shows axial images and 12 zoomed SS tumor parametric maps. Panels a and h display whole [one] breast image slices: 2 cm scale bars. Panel a and the upper 6 maps [b-g] are from a patient subsequently determined a non-complete responder by pathology [Non-pCR] after 18 weeks of NACT. Panel h and the lower 6 maps [i-n] are from a patient similarly judged a complete responder [pCR], RCB = 0. The top row [b-d, i-k] for each patient was obtained at TP_0, the bottom row [e-g, l-n] at TP_1, after only one 3 week NACT cycle [best estimates for image slice equivalence]. Thus, a comparison of a patient's TP_0 map with that at TP_1 shows the effect of the first NACT cycle. The Non-pCR patient [1a] is ER- and PR-negative, but with family history: her NACT comprised a Trastuzumab, Docetaxel, and Carboplatin cocktail, once/cycle. The pCR patient [1h] is ER- and PR-positive: her NACT comprised a Trastuzumab and Paclitaxel cocktail. The K^{trans} decrease [1i,l] for the pCR patient is dramatic. At the same time, τ_i increases [1k,n]. Importantly, the τ_i increase and K^{trans} decrease after 3 weeks NACT predict very well the RCB to be surgically found after 15 more weeks of therapy. This prediction bears up in ROI- and population-averaged results (4).

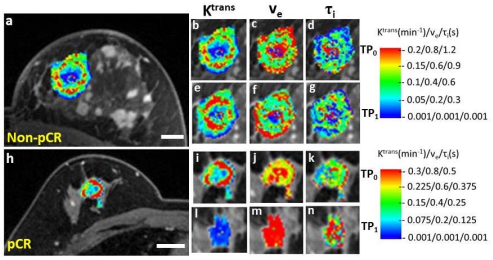

The maps exhibit significant intra-tumor heterogeneity that appears anatomic. For example, the TP_0 K^{trans} maps [1b, 1i] display elevated values in the tumor rim relative to the core: the variation exceeds 10X. Furthermore, there are often spatial correlations between imaging biomarkers. In the Fig. 1 K^{trans}/τ_i pairs [especially b/d and l/n, less so e/g and i/k], regions with relatively elevated K^{trans} generally have relatively smaller τ_i, and *vice-versa*. [The Non-pC core τ_i (1d) can be quite large, 1 s.] Cytoplasmic water is "well-mixed" (8): for a spherical cell, $\tau_i = 0.17(d/P_W)$, where d and P_W represent respectively the voxel *mean* cell diameter and cytolemmal water permeability coefficient (9). Thus, τ_i variations can reflect d variations, P_W^{-1} variations, or both. Consider the Non-pCR TP_0 τ_i map [1d]. τ_i values representative of the rim and core are 0.60 s and 0.81 s, respectively. We can use the corresponding v_e map [Fig. 1c] to estimate the rim/core d variation. The intracellular volume fraction [v_i] is approximated $(1 - v_e) \approx v_i \equiv \rho V$, where ρ is the cell number density and V the mean cell volume; and $d \sim V^{1/3}$. Using these relationships, and v_e values representative of the Fig. 1c rim and core [0.38 and 0.73, respectively], we find for a practical range of rim/core ρ ratios [0.8 to 1.4], the rim has larger d values than the core, by 18 to 43%. Since the tumor rim has smaller τ_i but larger d, τ_i must be dominated by the P_W factor: the rim has a larger P_W than the core. We compared the τ_i and v_e values of 21 pairs of *loci* within the 8 Fig. 1 maps [c,d,f,g,j,k,m,n]. For an average τ_i decrease of 44%, the average d change was 0%. This is consistent with independent estimated or measured d changes accompanying τ_i decreases caused by oxygenating yeast cells (9), treating acute myeloid leukemia [AML] cells with cisplatin (10), or comparing control *in vivo* mouse myocytes with those during chronic hypertension (11), **Table**. In every case, P_W increases. The τ_i biomarker magnitude is dominated by the mean cytolemmal water permeability coefficient, P_W.

	yeast	AML	myocyte	breast tumor
τ_i decrease	52%	79%	56%	44%
d decrease	7%	9%	23%	0%
ref.	9	10	11	this work

Discussion: The large τ_i value, 544 ms, in Fig. 1n obtains while v_e is also very large, 0.84 [2m]. If v_e is large, then v_i [$\approx 1 - v_e$] is small. As it should not [and contrary to what one might intuit], τ_i does not decrease with v_i: it reflects P_W. The P_W(passive) component [**Figure 2**] includes simple diffusion, passage through aquaporin channels, leakage through membrane proteins, *etc.*. However, the active trans-membrane water cycling, P_W(active), flux [10^{12} H_2O molecules/s/cell], dominates P_W(passive) (9). This is H_2O co-transport, *via* membrane substrate symporters, paced by the driving membrane ATPase pump; Na^+/K^+ATPase [NKA] for mammalian cells. The τ_i magnitude is sensitive to the ATP_i and K_o^+ substrates for, and specific inhibitors of, the driving ATPase transporters (9,12,13). Thus, τ_i is a reciprocal measure of on-going NKA activity. Before therapy, the responsive tumor has a rim that is relatively well perfused [large K^{trans} (1i)] and has relatively high NKA activity [small τ_i (1k)]. After 1 NACT cycle, the perfusion is drastically reduced [1l] and the activity concomitantly decreased, particularly in the residual core [large τ_i (1n)]. This is sensible, and seems provide a direct high-resolution view of the spatial, microenvironmental, and metabolic consequences of therapy.

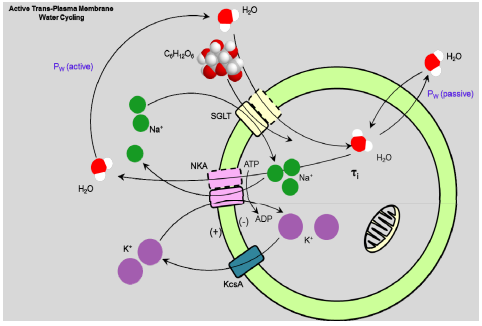

Grant Support: NIH: RO1-NS040801; UO1-CA154602; R44 CA180425.

References: **1.** Li, *et al*, *JMR* **218**:77-85 (2012). **2.** Huang, *et al*, *R* **261:**394-403 (2011). **3.** Li, *et al*, *MRM* **69:**171-178 (2013). **4.** Tudorica, *et al*, *PISMRM* **21:**504 (2013). **5.** Gerlinger, *et al*, *NEJM* **366:**883-892 (2012). **6.** Marusyk, Polyak, *S* **339:**528-529 (2013). **7.** Tudorica, *et al*, *MRI* **30:**1257-1267 (2012). **8.** Strijkers, *et al*, *MRM* **61:**1049-1058 (2009). **9.** Zhang, *et al*, *Biophys J* **101**:2833-2842 (2011). **10.** Bailey, *et al*, *MRM* **62:**46-55 (2009). **11.** Coelho-Filho, *et al*, *Circ* **128:**1225-1233 (2013). **12.** Poirier-Quinot, *et al*, *PISMRM* **14:**1176 (2006). **13.** Zhang, Balschi, *PISMRM* **21:**4045 (2013).